batteries

Article

Verification of the Modified Degradation Mode Identification Technique by Employing Electrochemical Impedance Spectroscopy and Differential Voltage Analysis

Sadia Tasnim Mowri *, Anup Barai, Aniruddha Gupta and James Marco

Warwick Manufacturing Group (WMG), University of Warwick, Coventry CV4 9AL, UK
* Correspondence: sadia.tasnim-mowri@warwick.ac.uk

Abstract: For retired automotive lithium-ion batteries, state of health (SoH) is currently utilised to grade them for a second-life application. However, researchers previously challenged this and expressed that, in addition to SoH, the actual degradation mechanism, also known as degradation mode (DM), should be considered for grading, for efficient second-life operation. To date, there is little evidence to support this. A validated DM detection technique for cell/module grading does not exist. A modified DM detection technique by tracking and indexing the incremental capacity (IC) curves was previously proposed by the authors; nevertheless, it was difficult to validate. Researchers previously proposed DM identification using Electrochemical Impedance Spectroscopy (EIS) and Differential Voltage (DV) analysis. With a direct comparison of the techniques made exploiting IC, DV, and EIS, a correlation can be made, which is presented in this article. The correlation suggests that cells identified as having the same (or different) DM by the proposed technique also identified as having the same (or different) DM growth by EIS technique proposed by other researchers. Likewise, DV analysis suggests that the DV peak's standard deviation of similar DM cells is smaller than that of the different DM cells.

Keywords: second-life of lithium-ion battery; IC-DV curve; EIS; DM identification; cell grading

Citation: Tasnim Mowri, S.; Barai, A.; Gupta, A.; Marco, J. Verification of the Modified Degradation Mode Identification Technique by Employing Electrochemical Impedance Spectroscopy and Differential Voltage Analysis. *Batteries* **2022**, *8*, 274. https://doi.org/10.3390/batteries8120274

Academic Editor: Juan Carlos Álvarez Antón

Received: 6 October 2022
Accepted: 28 November 2022
Published: 5 December 2022

1. Introduction

Introducing Electric Vehicles (EVs) and Hybrid Electric Vehicles (HEVs) is considered a step toward a greener world and the decarbonisation of the transportation sector [1–3]. UK car-registration data suggest that the registration of the EVs and HEVs increased by 88% and 43%, respectively, in 2022 from 2021 [4]. In 2018, the increase was 20% from 2017 for alternative-fuel vehicles (e.g., HEV, EV, fuel cell) [5]. These statistical data demonstrate that sales of EVs have increased rapidly in the last few years.

A total of 20 million EVs are anticipated to be operational in Europe by 2030, and more than 100 million by 2040 [6]. An extensive number of batteries will be phased out of initial automobile use as the quantity of EVs increases. As a result, a circular economy structure, including retired batteries is essential. Within a circular-economy scenario, all the batteries should be recycled when they reach their end of life. However, for a retired EV battery, there are various alternatives, including recycling straightway [7], reusing without significant changes in a different application before recycling [8], and reusing through remanufacturing [9]. The use of retired batteries through remanufacturing or reusing (pack/module) without major changes is usually known as their second life. However, not all the batteries retired from the automotive application are suitable for second-life applications [3]. Typically, a battery's eligibility for second-life application is determined by estimating the maximum capacity of the battery at the time of retirement, also known as the state of health (SoH). In addition to capacity, SoH assessment often consists of battery-internal-resistance measurement [10,11].

For a particular pack/module, the decision of reusing without major changes or recycling can simply be made based on SoH. Often, the financial costs [12] may contribute to this decision. In contrast, a much more complex process needs to be followed for the reusing through remanufacturing. A remanufactured battery pack is assembled by retired cells/modules in series/parallel configuration. Thus, the capacity, power capability, and remaining life of the cell/module should be similar in a remanufactured pack [13]. This is to avoid pack imbalance and degradation gradients throughout the second life. The present technique of utilising SoH might be partly valid in determining the cell/module's eligibility for remanufacturing. It was previously stated in [14,15] that SoH as a metric is insufficient to provide a decisive answer on the current status of the battery. Previously Barai et al. [14] and Dubarry et al. [15] highlighted concerns about the requirement of degradation-mode (DM) (c.f Section 3) identification while grading the cells/modules for remanufacturing.

How battery cells will degrade in a second-life application could be related to how they degraded in first-life application, i.e., first-life DM. Cells could degrade at different rates in a second-life application when exposed to the same usages conditions i.e., temperature, charge-discharge current, solely because of their first-life DM was different. However, it is not proven yet. The authors of this article are currently performing experiments to generate data for this. Current DM identification techniques, such as pseudo-open-circuit voltage (pOCV), electrochemical impedance spectroscopy (EIS), and incremental capacity and differential voltage (IC-DV) can correlate battery degradation to their physical changes to active and inactive components at both electrode and electrolyte but are not suitable for grading of retired battery cells/modules based on degradation mode. Therefore, a modified DM identification technique for the cells/modules should be developed. Mowri et al. [16] proposed a modified DM identification technique which might be suitable for cell grading. In this article, the modified technique is applied to 22 cells, and an experimental correlation of the modified technique with EIS and DVA is also presented.

The contribution of this paper is the verification of the modified DM identification technique with other non-invasive processes (i.e., EIS and DVA). In short, we aim to determine if there are any similarities between the impedance variation and the DV curve of the cells that have been identified as the same DM cells. Alternatively, we intend to discover if there are any dissimilarities between the impedance variation and the DV curve of the cells that have been identified as different DM cells. EIS data were gathered to observe resistance variations in each group to corroborate the cell-grouping procedure. Moreover, DV curves are also analysed to get a correlation with the IC curves for each cell group.

The layout of this article is as follows: Section 2 defines the capacity-measurement technique. Section 3 explains the DM, introduces the existing DM detection techniques (EIS, IC, and DV), and describes the modified DM detection technique. Section 4 presents the experimental setup and methodologies employed for this research work. Using the capacity-measurement approach described in Section 2 and the modified DM detection technique described in Section 3, Section 5 identifies the SoH and DM of the cells. Section 6 correlates the EIS and DV curve data with the DM of the cells identified by IC curve. Further works are presented in Section 7. The conclusion of this investigation is described in Section 8.

2. Capacity Measurement

As highlighted in Section 1, while remanufacturing a pack, overall ageing status of the retired cells need to be same to avoid the pack imbalance. Additionally, Section 1 highlighted that the overall ageing status of a cell might not be determined by the first-life SoH alone. There might be some other contributing factors e.g., DM status [14,15]; however, effect of DM on a remanufactured pack/module for second-life application has not been proven yet. It was hypothesised that both SoH and DM of the cells represent the overall ageing status of the cells. In short, it is anticipated that when the SoH and DM of the retired cells in a remanufactured pack are similar, it performs best in second-life

application. Therefore, both DM and SoH need to be identified at the end of first life. According to current practice, capacity or resistance measurement ensures the SoH of the cells. Equations (1) and (2) show the most common method of defining SoH in terms of changes in energy capacity and resistance. Equation (1) is used here to estimate the SoH of the cells. The nominal capacity ($C_{nominal}$) of a battery is the capacity guaranteed by the manufacturer for a new cell operating under nominal conditions, such as nominal temperature (e.g., 25 C), nominal discharge current (e.g., one-hour discharge rate (1C)), and being fully discharged from a fully charged state [17], whereas the capacity of a particular battery cell under different operating circumstances will vary. It is referred to as the actual capacity (C_{actual}), which will vary at different operating and ageing states [17]. Similarly, nominal resistance ($R_{nominal}$) is the resistance value guaranteed by the manufacturer under nominal conditions, and SoC Resistance rises as battery degrades, therefore, R_{actual} is expected to increase over the battery lifetime.

$$SoH_c = C_{actual} / C_{nominal} \quad (1)$$

$$SoH_r = R_{actual} / R_{nominal} \quad (2)$$

SoH of the cell can be estimated by tracking the capacity or resistance of the cells. In general, a battery reaches the EoL when capacity is 0.8 times its initial value, or resistance is two times its initial value [18]. Previous data [19,20] suggest that resistance rises slowly in contrast to capacity loss at the earlier stage of battery life. In the early stages of a battery's life, capacity testing can detect degradation and offer more reliable data in comparison with resistance estimation. Therefore, for this research project, the SoH of the cells is estimated by employing the capacity test.

3. Assessment of Battery Degradation Mode

A multitude of electrochemical mechanisms causes the Li-ion cell to degrade. Many operating conditions, such as temperature, pressure, state of charge, discharge current, [21,22], influence and accelerate the degradation of Li-ion cells. Due to the significant interaction and dependency of degradation modes, it is difficult to attribute all of the causes to a single source of degradation. In order to ease the comprehension of the degradation manner, Dubarry et al. [23], Birkl et al. [24], and Marongiu et al. [25] recommended categorising them into three different groups: loss of active material (LAM), loss of lithium inventory (LLI), and conductivity loss (CL). The deterioration caused by binder dissolution or corrosion of the current collector is linked to CL [22]. Li-ions intercalate and de-intercalate from electrodes during the charge/discharge process store and distribute electrical charges within the cell. The loss of these lithium ions defines LLI [22]. Changes in the structure of the positive and negative electrode components permit lithium intercalation and de-intercalation, i.e., the formation of active materials. LAM primarily defines loss of the active material and electrolyte components [22]. Uddin et al. [21] and Vetter et al. [22] established the correlation between degradation causes and the most relevant DM. A critical review of DM detection is provided in Section 3.1.

3.1. DM Detection

Several approaches identify the DM of the cells, such as pOCV, EIS, Incremental Capacity (IC), and Differential Voltage (DV) analysis of pOCV [26]. Usually, DM is identified from the IC-DV curve by observing the changes in the IC and/or DV curves' peaks and plateaus, respectively. Table 1 [15,23,27] depicts the relationship between changes in IC-DV curves and the most relevant DM. To visualize the information provided in Table 1, the graphical image can be found in [26,27].

Table 1. Changes of the IC -DV curve with respect to DM.

Changes in IC Peak	Unit	Changes in DV Peak	Unit	DM
Shrinkage of the magnitude of the peaks along with the shifting in the direction of higher voltages	[AhV^{-1}] and V	Shifting of the DV curves in the direction of the lower capacities without shifting of the DV peaks	[Ah]	LLI
Shifting of the peaks in the direction of the lower voltages	V	Insufficient change	[Ah]	CL
Shrinkage of the magnitude of the peak at a nearly persistent voltage	[AhV^{-1}]	Shifting of the DV curves in the direction of the lower capacities	[VAh^{-1}]	LAM

EIS is a widely recognised method for measuring the impedance of a cell over a wide frequency range (mHz to kHz). In addition to measuring the cell's internal resistance, the EIS test can identify the DM. Pastor-Fernández et al. [28] attempted to establish a link between the resistances of the equivalent circuit model (ECM) and the DMs. In this method, ECM resistances are monitored to identify and quantify the most relevant DMs [28]. In that proposed technique, current collectors, connectors, and electrolyte resistance are represented by R_{ohm} [29]. CL is caused by corrosion of current collectors and connections, as well as changes in electrolyte decomposition caused by side reactions. As a result, the rise in R_{ohm} may be used to quantify the rise in CL. One of the most important ageing mechanisms in Li-ion batteries is solid electrolyte interface (SEI) (formation, build-up, and disintegration). SEI prevents Li-ion intercalation and de-intercalation between the electrolyte and the negative electrode. This interphase, in turn, causes irreversible Li-ion consumption (LLI), resulting in significant capacity loss and increased resistance [23]. Therefore, the rise in R_{sei} is a result of LLI. Besides the SEI, LLI is responsible for additional degrading effects, such as dendritic development and micropore clogging. From the aspect of the cell's voltage-response dynamics, these effects and SEI are interpreted as a decrease in the charge-transfer Li-ion intercalation and de-intercalation processes [23], which manifests as an increase in the charge-transfer resistance, R_{ct}. Consequently, the rise in R_{ct} is likewise a result of LLI. This indicates that LLI is associated with several resistances, R_{sei} and R_{ct}. Different concentration levels within a Li-ion particle result in diffusion. This results in structural changes inside the Li-ion particle and between Li-ion particles [11,23,30]. A Warburg impedance, Z_W, models the diffusion processes. Warburg resistance, R_w, is dependent on the diffusion path length. Since diffusion processes are associated with formation changes in the electrode structure, LAM may be primarily responsible for the rise in R_w. Table 2 displays the association between ECM resistance and the most relevant DMs.

Table 2. The relationship between ECM resistance and the most pertinent DMs [27].

ECM-Component	Unit	Most Relevant DM
Growth of R_{ohm}	[Ω]	CL
Growth of R_{sei} & R_{ct}	[Ω]	LLI
Growth of R_w	[Ω]	LAM

To quantify the effects of DMs over cycle number, a parameter-termed growth in percentage is proposed in [27] to calculate the %LLI and %LAM following equations are proposed in [27].

$$\mathbf{LLI_{EIS,x,n}}\ (\%) = \frac{(\mathbf{R_{SEI,x,n}} - \mathbf{R_{SEI,1,n}}) + (\mathbf{R_{ct,x,n}} - \mathbf{R_{ct,1,n}})}{\mathbf{R_{SEI,1,n}} + \mathbf{R_{Ct,1,n}}} \cdot 100 \tag{3}$$

$$\mathbf{LAM_{EIS,x,n}}(\%) = \frac{(\mathbf{R_{W,x,n}} - \mathbf{R_{W,1,n}})}{\mathbf{R_{W,1,n}}} \cdot 100 \tag{4}$$

Here, X = no. of characterisation and n = no. of cell

According to Tables 1 and 2, the DM of the cells might be detected using IC-DV and EIS, respectively. Table 2 presents the most relevant DM that correlates with the growth in the ECM component. However, unlike Table 2, Zhu et al. [31] suggested that R_{ohm} demonstrates a rising trend with LLI. An identical variation may also be observed on the R_{sei}. This phenomenon can be explained by the production of new SEI through the consumption of mobile lithium and electrolyte. The rise in R_{sei} reflects the accumulation of SEI, while the increase in R_{ohm} is attributable to electrolyte deficiency. Zhu et al. [31] also suggested that an increase in R_w is mainly related to cathode loss. However, R_w has a strong mathematic relationship with LLI. However, there is hardly any validation data in support of the relationship of the most pertinent DM with the ECM component. Thus, DM detection using the EIS is still an immature approach, and further study is required in this field.

Typically, ageing increases the resistance of any given cell. Consequently, if Table 2 is applied to aged cells, it is probable that their ECM component (R_{ohm}, R_{sei}, R_{ct}, and R_w) will be found to be increased. If every ECM resistive component is increased, the cell's most relevant DM will be a combination of LLI, LAM, and CL. Therefore, if Table 2 is applied to the number of aged cells, it is likely that the most relevant DM for the number of aged cells will be a combination of LLI, LAM, and CL [27,28]. If the DM of the number of aged cells is a combination of LLI, LAM, and CL, it is hard to categorise cells based on their DM in their first life. Therefore, Table 2 is acceptable for detecting DM but not for grouping cells according to their DM.

Keil et al. [32] employed the half-cell data to identify the DM from the DV curves. In that process, DM is identified from the shifting of the DV curve from a new condition to an aged condition. This process can identify the overall DM of the cell. Previous literature suggests that there is hardly any cell containing only LLI/LAM/CL. In most cases, DM of the cells is a combination of LLI and LAM, or LLI, LAM, and CL [15,23,33–35]. Therefore, if the overall DM of a cell is identified, it would be a combination of LLI and LAM, or, LLI, LAM, and CL. The limitation of DVA with half-cell data is that it can identify a cell's overall DM. It is challenging to categorise cells based on their DM in their first life only by identifying the overall DM of the cells.

Alternatively, DM of the individual valley of the DV curve can be identified by employing the relationships in Table 1. Nonetheless, the issue with this process is that DM is identified from the plateaus of the DV curves in that process. As plateaus are flat regions, it is difficult to identify the shifting of the individual plateaus, as shown in Figure 1a. Magnification of DV curves reveals comparatively prominent DV plateaus (refer to Figure 1b). The magnified plateaus are still shallow in comparison with the IC peaks, as shown in Figure 1c. Using these shallow DV peaks, it is difficult to identify the shifting and decreasing of the individual plateaus DV curves. Hence, DV curves are less traceable than IC curves. Thus, among these three non-invasive techniques, IC curve is used in this article to identify the DM of the cells.

This article identifies DM from the IC curves by observing the peak changes, as mentioned in Table 1. Currently, IC curves are widely used for DM identification [23,25,27]. An IC curve can be achieved by differentiating the Q with respect to the p-OCV. The results from Dubarry et al. [15,23] and Pastor et al. [27] are used to identify the DMs using full-cell IC curves.

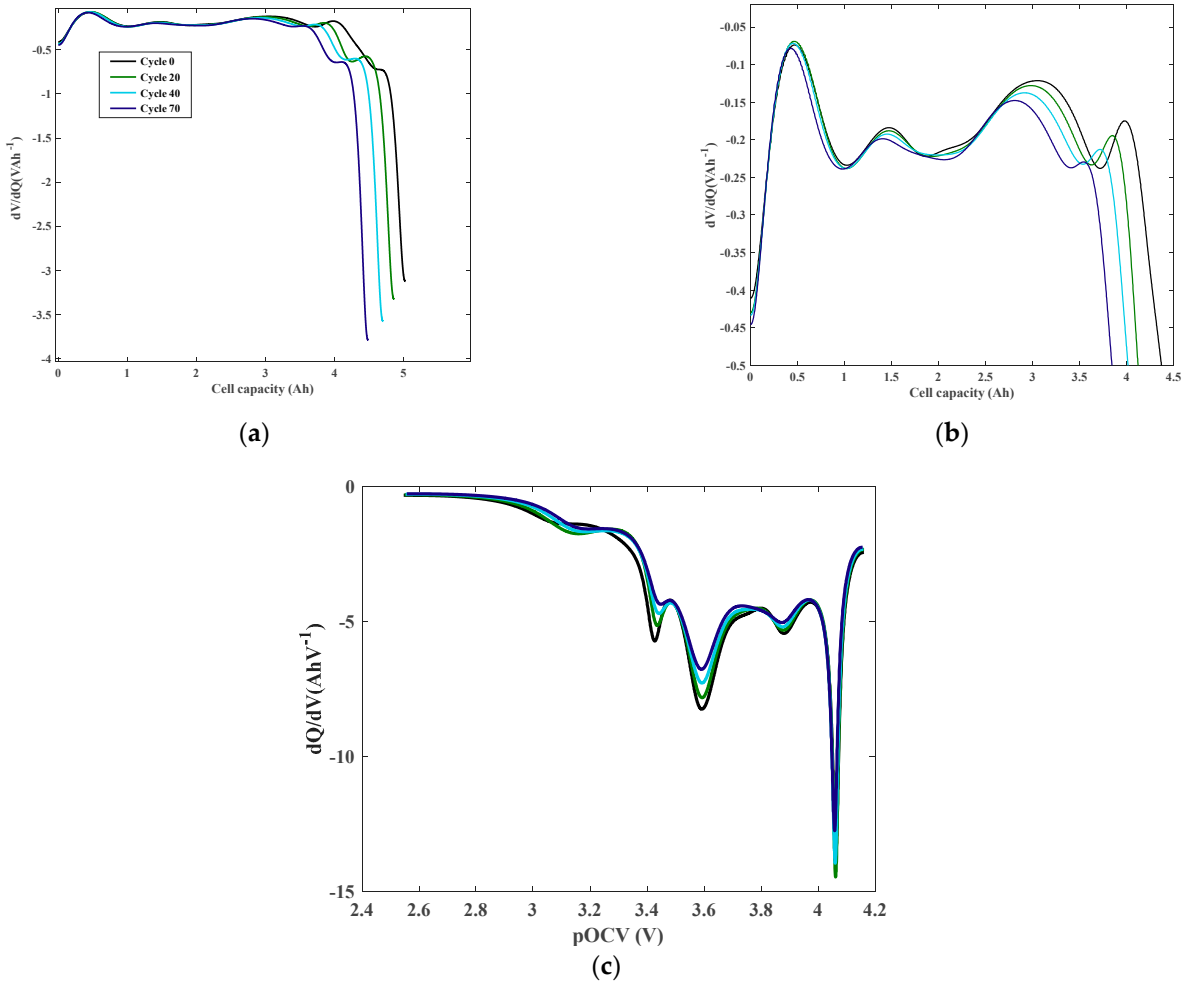

Figure 1. IC-DV curve of Cell L (**a**) DV curve. (**b**) magnified view of the DV curve. (**c**) IC curve.

To perform DM identification from IC, the origin of pOCV, OCV, and resistance needs to be understood. It has been explained a number of times before, such as in [14], but a short explanation is provided below. In simple terms, pOCV (V_{pOCV}) can be derived from the difference between pure open circuit voltage (OCV), V_{oc}, and the voltage drop due to R_{ohm} as given in Equation (5) [27].

$$V_{pOCV} = V_{oc} - V_{ohm} = V_{oc} - I.R_{ohm} \quad (5)$$

Usually, R_{ohm} represents the resistance of current collectors, electrolytes, and connections [29]. CL occurs due to the corrosion on components, such as current collectors and connections, along with side reactions that alter the electrolyte composition. CL elucidates voltage drop with R_{ohm}. As a result, the rise in R_{ohm} may be used to quantify the increase in CL [27]. However, Equation (5) provides a constant V_{oc} and I; if R_{ohm} increases, V_{pOCV} decreases. As mentioned previously, the rise in R_{ohm} is connected to the growth in CL. This implies that an increase in R_{ohm} has no effect on the cell's capacity, whereas cell voltage is affected by this resistance increment [23,27]. Thus, in the absence of capacity fading, the impact of CL may be shown as a shift of the IC curve toward lower voltages [23,27].

SEI is one of the leading causes of ageing, which leads to LLI and is responsible for capacity and power fading. When the electrolyte and anode are in contact, SEI prevents Li-ions from being intercalated and de-intercalated. The irreversible depletion of Li-ions occurs as a result of this interphase (LLI) [27]. Thus, the rise in R_{sei} is a result of LLI. In addition to SEI, lithium dendrite or micro pore-clogging are also responsible for LLI. In terms of the cell's voltage response, lithium dendrite or micro pore-clogging and SEI together decrease

charge-transfer Li-ion intercalation and de-intercalation reactions, resulting in an increase in R_{ct} [27]. Reduced charge-transfer Li-ion intercalation and de-intercalation reactions result in a drop in V_{oc} and charge (capacity). This is visible in the IC peaks as a reduction in peak heights along with a move toward lower or higher voltages, respectively (IC) [27].

A drop in the amplitude of the IC curve's peaks indicates a decrease in the charge at approximately constant V_{pOCV}. V_{pOCV} shifts minimally in this situation, indicating that the system is approaching equilibrium and that the total overpotential is near zero [27]. The movement of a small number of Li-ions is involved in this scenario from an electrochemical perspective, and as a result, the majority of the phase shifts are ascribed to the disordering of the active materials' structural properties (LAMs) [23,36].

3.1.1. Modified DM Identification Technique

As it is not possible to utilise the relationships in Table 1 to group the cells based on their DM, a modified DM identification technique was proposed in [16], and a summary of the modified DM identification technique is given below.

DM of the cells is identified by following the shifting and decreasing of the IC peaks. After plotting a number of IC curves in the same plot in [16], it is noticed that all peaks are shifting along the x-axis by a few mV, while their intensities are altering along the y-axis by a few $mAhV^{-1}$. Hence, it is difficult to get a number of IC peaks which are exactly at the same position. To overcome these challenges and differentiate the evolution of DM, selection of a threshold point is required.

In [16] 5 mV (abscissas) or 5 $mAhV^{-1}$ (ordinates), the peak-position difference is taken as the threshold point to perveivethe changes of the IC peaks. It is assumed that 5 mV or 5 $mAhV^{-1}$ deviation is insignificant and can be considered almost negligible, and peaks with a 5 mV difference can be considered constant. Jia et al. demonstrated in [37] that as long as the difference between two cells' OCVs is less than 6 mV, the difference has a negligible effect on the cells' OCV-SoC or OCV-Capacity curves. This indicates that a 5 mV difference in OCV has no discernible effect on the OCV-capacity curve. If the OCV-capacity curves are identical, the IC curves generated by the OCV-capacity curves should also be identical. Thus, the 5 mV difference between the peaks of two IC curves can be treated as a constant voltage; it has a negligible effect on ageing and can be ignored. 6 mV can be selected as a threshold point. Nonetheless, instead of 6 mV, 5 mV is selected here to minimise the measurement error. To determine the impact of altering the 5 mV, a statistical study was conducted on around 430 IC peaks. The study shows that, if the limit is dropped to 4 mV, 7% of peaks change their DM status (which was identified with 5 mV limit), and if the limit is increased to 6 mV, approximately 4.5% of peaks change their DM status. Hence, the research reveals that changes of ± 1 mV in the limit value will not significantly affect the existing result. Following the relationship in Table 1, two conditions are assumed in the modified DM identification technique:

Assumption 1. *If the difference between horizontal-axis peak points (i.e., ① and ② from Figure 2b) is ≥5 mV, peaks are shifted. If the difference is <5 mV, then it is considered that peaks are not shifted, i.e., peaks are at a constant voltage* [16].

Assumption 2. *If the difference between vertical-axis peak points (i.e., ③ and ④ from Figure 2b) is ≥5 $mAhV^{-1}$, peaks are reduced. If the difference is <5 $mAhV^{-1}$ then it is considered that peaks are not reduced* [16].

① & ② represent the horizontal position of the IC peaks. Figure 2b reveals that difference between ① & ② is 31.55 mV (i.e., 4th IC peak is shifted by 31.55 mV) after cycle 600. Inversely, ③ & ④ delineate the vertical position of the IC peaks. The difference between ③ & ④) is 1372.5 $mAhV^{-1}$, which indicates that IC peak decreased by 1372.5 $mAhV^{-1}$. The changes of the IC peak display, the 'peak shift' is greater than 5 mV also 'peak decrease' is >5 $mAhV^{-1}$. As P-4 is both shifted and decreased; thus, according to Table 1, it is believed that P-4 is LLI dominated.

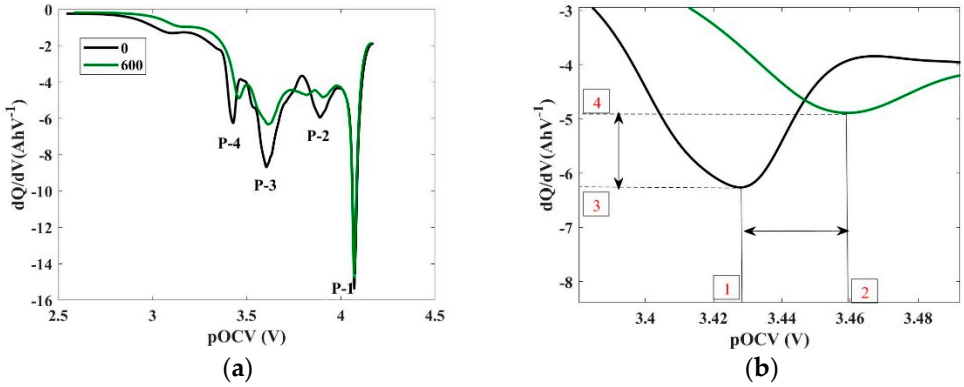

Figure 2. IC curve of a cell (**a**) at new (0 cycle) and aged (600 cycle) condition (**b**) magnified 4th IC peak (P-4). Adapted from [16].

Although P1–P4 might be labelled either as LLI or LAM, it is likely a mix of LLI and LAM. However, by labelling a peak as LLI or LAM, it is inferred that LLI or LAM is dominant for that peak. This simplification allows implementation of DM (or dominant DM) for cell grading. To reiterate, the primary objective of this research is to identify a group of cells at the same ageing stage. Same ageing state can be ensured by maintaining a similar SoH level and IC curve pattern [14,15]. If the IC curves are identical, it is assumed that the degradation is identical; if they are not identical, the degradation is different [14]. IC curves consist of a similar peak number, position, and similar peak changes might be considered identical. The number and position of any IC peak are visible from the IC curves. Therefore, tracking the changes in IC peaks makes it possible to identify the identical IC curves [15,23,35]. Henceforth, it is believed that similar changes in the IC peak may represent the similar DM of the IC peaks. Table 1 provides the most pertinent DM of the cells based on the changes in the IC peaks. Thus, it was hypothesised that IC curves consisting of similar IC peak position, number, and DM might be identical. Alternatively, IC curves consisting of different IC peak positions or numbers or DM might be different. By using the above technique, the cells identified as same DM cells surely share similar a SoH level, IC curve, and eventually the same ageing pattern.

A comparison of the modified DM identification technique with other techniques is given in Table 3, which shows that DM was identified through visual inspection in the previous DM identification method [11,13–15]. Through visual inspection, it would be hard to quantify the DM of the cells via the previous method. In contrast, DM is identified in the modified DM identification technique by measuring the difference between the IC peaks at aged and new conditions. Therefore, the modified DM identification technique will probably be used to grade the cells.

Table 3. Comparison of modified DM identification technique with other techniques.

Characteristics	Dubarry Method	Carlos Method	Modified DM Identification Method
Definition of DMs	LLI, LAMde^{PE}, LAMli^{PE}, LAMde^{NE}, LAMli^{NE}	LAM, LLI and CL	LAM, LLI and CL
Assumption of DM	From IC peak change	From IC peak change	From IC peak change
Detection of IC peak change	Visual Inspection	Not Defined	Measurement of the IC peak positions at the new and aged condition
Suitable for cell grading	Not Defined	Not Defined	Could be used for cell grading

The DM identified using the modified DM detection technique requires further investigation for verification. The verification can be done by employing the post-mortem analysis technique or applying any other non-invasive techniques which can identify DM of the cells. Post-mortem techniques range from scanning electron microscopy (SEM), X-ray diffraction (XRD), to X-ray fluorescence (XRF). However, all the techniques provide information regarding the physical changes of the cells. For example, SEM images provide useful information on the microstructure dynamics in the battery electrode. In combination with other methods, SEM can provide significant information for determining the surface-degradation processes of this material. SEM was used to investigate the formation of the solid electrolyte interface (SEI) on the surface of graphite particles during ageing [38,39]. The electrolyte dissolution that occurs with age and the growth of the SEI is the cause of Li loss and, consequently, a decrease in capacity [38–41]. XRD peaks provide information about the material compounds and phases formed during the charging and discharging of the batteries. XRD has been widely employed in diagnosing degradation mechanisms because it gives information on the structural changes that active crystalline materials can undergo during ageing [39,42,43]. Post-mortem techniques can correlate the DM identified with the physical changes to the electrode materials. However, most post-mortem findings cannot provide temporal resolution and relationship with the underlying process. Moreover, the assessments are sometimes equivocal on cause-and-effect development (due to the absence of a temporal relationship), which may result in path-dependent deterioration [44]. Other non-invasive techniques, such as DVA or EIS, can verify the DM of the cell. However, these techniques lack the ability to generate evidence of the physical correlation between the cells and have their limitations, as explained earlier. As the authors intend to expose these cells to further degradation using a second-life duty cycle, instead of destructive post-mortem analysis, other non-invasive techniques, i.e., DVA and EIS, are used here to verify the DM of the cells.

4. Experimental Details

The experiment in this study investigates the DM of the individual cells. The overall test of ageing consists of two stages.: the constant cycling (c.f. Section 4.2) and the reference performance test (RPT) (c.f. Section 4.3). Cells were continuously charged-discharged using different current rates under a constant-cycling step. Individual cells were subjected to a set of experiments named the RPT prior to beginning the cycling procedure and the constant-cycling interval. The following sections present the experimental setup, charge-discharge process, and RPT.

4.1. Cell Specification and Experimental Setup

A total of twenty-two commercially available lithium-ion LGM 50 cylindrical 21,700 format cells were used in this experiment. The rated capacity of the individual cell was 5 Ah, which consists of the NMC 811 positive electrode and bi-component Graphite-SiOx negative electrode. The standard charge and discharge voltage are 4.2 V and 2.5 V, respectively. The cells were denoted as Cell A, Cell B, Cell C . . . . . Cell V, respectively.

To perform testing of the individual cell, both positive and negative terminals of the cells were spot-welded with aluminium tabs. During both constant cycling and RPT, cells were submerged in a liquid cooling bath at a constant temperature of 25 °C. The liquid–cooling bath provided active cooling, which was essential to maintain the temperature at 25 °C. All charge-discharge was conducted employing a commercial Digatron battery cycler (MCT 10-6-192 HD). A schematic and real picture of the experimental setup is shown in Figure 3a.

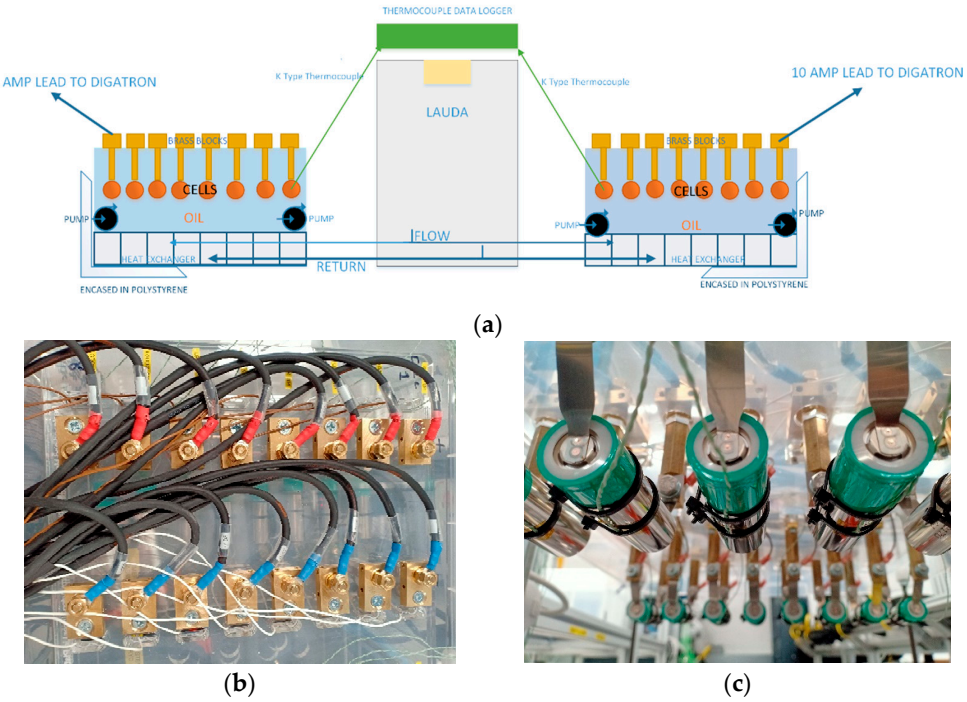

Figure 3. Experiment setup (**a**) the schematic diagram. (**b**) top view of the real setup. (**c**) cells inside the setup.

4.2. Ageing Test

The flowchart of the test is illustrated in Figure 4. At the beginning of the ageing test, RPT of the individual cells (new condition) was performed. Following that, a number of constant current charge-discharge cycles were performed (the number of cycles varied for different cycling conditions shown in Table 4, after which RPT of the cells was done. This process was repeated until the cells reached 80% SoH.

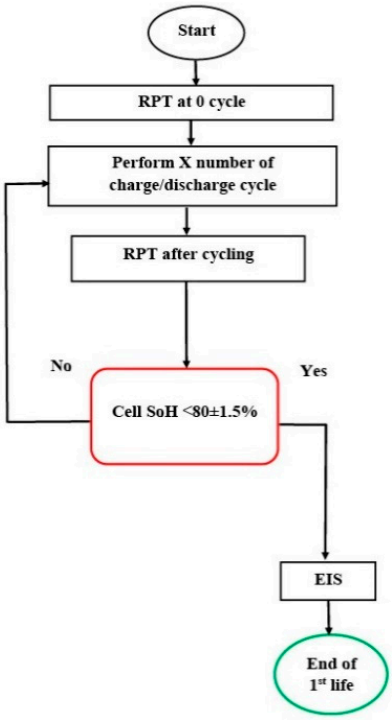

Figure 4. The progression of the ageing test of the individual cell.

Table 4. Test matrices of this experiment.

Sl No	Cycling Condition (Ch-Dch)
1	0.5C_1C
2	0.7C_0.3C
3	0.7C_0.5C
4	0.7C_1C
5	0.7C_1.5C

For constant-current cycling, cells were charged using the constant current–constant voltage (CC-CV) procedure, then discharged using a constant current. The charge-discharge current rates for five-cycling conditions are illustrated in Table 4, and the temperature during cycling was 25 °C. During charge, the cells were charged to 4.2 V using a constant current and then in the CV step, when the current dropped below C/20 (0.25 A), charge was stopped. After an hour of rest, cells were discharged at their respective rate (e.g., 0.3C/0.5C/1C/1.5C) until the cell voltage dropped to 2.5 V. After discharge, another one-hour rest period was added before the charge-discharge process was repeated. Initially, it was expected that cells cycled with different C-rate might provide different DM. Hence, cells were cycled with five different C-rates to reach the end of their first life (80% SoH).

4.3. Reference Performance Test

The RPT of the cells was performed at 25 °C. RPT consists of a capacity test using C/3 current and a pOCV test using C/10 current. Prior to the capacity test, cells were initially charged by following CC-CV approach, where C/3 current is employed for the CC phase to 4.2 V and C/20 cut-off current at the CV phase. For capacity test, cells were discharged to 2.5 V using C/10 current, then charged to 4.2 V using C/10 current. Then, cells were again discharged using 1C to 2.5 V and charged using 1C to 4.2 V. There was a 1 h rest period between every charge and discharge step. Data from the C/10 discharge step are used to derive the incremental capacity (IC) curve.

4.4. Electrochemical Impedance Spectroscopy (EIS)

To understand the change of impedance, and verify DM, EIS of the cells was done when cells were new and when they reached 80% SoH. EIS tests were performed at 50% SoC at 25 °C. The SoC adjustment was made by employing a commercial cell cycler (Maccor) and an environmental chamber (Espec). The adjustment protocol includes charging the cell to the manufacturer-defined charge voltage (4.2 V, defined as 100% SoC). After charging, a one-hour rest period is applied. Then, cells are discharged employing 1C current until 3.6 V is reached (50% SoC). Another four-hour rest time was included to allow the cells to achieve electrochemical equilibrium. After that, EIS was performed on the cells.

5. Results

5.1. SoH Measurement

In general, an EV battery reaches the first EoL at 70–80% of its initial capacity [3,45,46]. Hence, this article considers 78 ± 1.5% to 80 ± 1.5% SoH to be the end of the first life. Nonetheless, it is unlikely to get a group of cells precisely at the same SoH. SoH of the cell could vary due to measurement error or cell-to-cell variation. Numerous articles have been published in which researchers acknowledged an error margin of 1–2% [10,47] when determining the SoH of cells. Thus, a margin of ±1.5% is employed in this article. Equation (1) is used here to calculate the SoH of the cells at the end of their first life. SoH of the cells is provided in Table 5.

Table 5. DM of the cells.

Cell	P4	P3	P2	P1	SoH%
Cell A	LAM	LLI	LAM	LLI	80.58
Cell B	LAM	LLI	LAM	LLI	80.54
Cell C	LLI	LLI	LAM	LLI	79
Cell D	LAM	LLI	LAM	LLI	81.16
Cell E	LAM	LLI	LAM	LLI	78.76
Cell F	LAM	LLI	LAM	LLI	77.56
Cell G	PD (Peak Disappeared)	LLI	LAM	LLI	78.58
Cell H	LAM	LLI	LLI	LLI	79.35
Cell I	LLI	LLI	LLI	LLI	78.51
Cell J	PD	LLI	LAM	LLI	81.56
Cell K	LAM	LLI	LAM	LLI	79.14
Cell L	LLI	LLI	LLI	LLI	76.95
Cell M	LLI	LLI	LLI	LLI	78.56
Cell N	LLI	LLI	LLI	LLI	78.4
Cell O	LLI	LLI	LLI	LLI	76.75
Cell P	LAM	LLI	LLI	LLI	77.96
Cell Q	LAM	LLI	LLI	LLI	78.36
Cell R	LAM	LLI	LLI	LLI	79.74
Cell S	LAM	LLI	LLI	LLI	76.95
Cell T	LAM	LLI	LLI	LLI	79.76
Cell U	PD	LLI	LLI	LLI	80.76
Cell V	LAM	LLI	LLI	LLI	80.56

Though the SoH of the cells is almost (±1.5%) identical, their ageing status may differ, as discussed in Section 1. SoH of a cell only represents the capacity degradation of the cells; it does not reflect the causes that underpin the degradation [15]. Therefore, a more systematic approach is required to decipher a change in the physical processes of the cells. This can be done by identifying the DM of the cells. However, the DM detection methods that are now in use are not intended to grade the cells or module after their first life. Henceforth a modified DM detection process is proposed in [16]. Applying the modified DM detection technique, DM of the cells given in Table 5 are identified.

5.2. DM Detection

DM is identified by employing Table 1 and following the process described in Section 3.1.1. The identified DM is given in Table 5, and the corresponding IC curves of the cells are shown in Section 6.2. In Table 5, P1, P2, P3, and P4 represent the 1st, 2nd, 3rd, and 4th peak positions of the IC curves, respectively, as shown in Figure 2a.

The experiment was designed to get the cells at the same SoH level. After getting a similar SoH level, DM of the cells is identified. According to a prior investigation [16], when each peak of each cell of the IC curve is resembled, the cells are in the same DM state; however, when the circumstances are opposite, the cells are in a different DM state. The same DM and different DM cell groupings are formed based on those conditions. Table 5 provides that IC peaks of the Cell A, B, D, E, F and K are similar. For all these six cells (Cell A, B, D, E, F), 4th IC peak(P4) = LAM, 3rd IC peak (P3) = 2nd LLI, 2nd IC peak (P2) = LAM and 1st IC peak (P1) = LLI. The peaks for all these six cells are similar; thus, these six cells are considered the same DM cells. Likewise, Table 5 depicts that four IC peaks are similar for Cell H, P-T & V (P4 = LAM, P3 = P2 = P1 = LLI) and Cell L-O (P4 = P3 = P2 = P1 = LLI).

Table 5 also depicts that IC peaks of the Cell G, K and U are different. Among these three cells (Cell G, K, and U), P3 & P1 = LLI for all three cells. Alternatively, P4 = PD is observed for Cells G and U, whereas P4 = LAM is noted for Cell K. Furthermore, P2 = LAM is recorded for Cells G and K, while P2 = LLI is observed for Cell U. The above analysis shows that, for Cells G, K, and U, two peaks (P3 & P1) are similar for all three cell. Nonetheless, there are variations between P4 and P2 among the three cells. A previous study [16] suggests that, if the peak of each cell is not matched, the cells might be in at

different DM state. Thus Cell G, K, and U are considered as different DM cells. Likewise, Cell C, D, J, and I are also considered as different DM cells. Though SoH and DM of the Cell A, B, D, E, F, and K are similar, Cells A, B, E, and F are the members of the same DM cell group; Cells D and K are used to make different DM cell groups.

The groups which consists of the same and different DM cells are denoted as cell same (CS) and cell different (CD). The three same DM cell groups are denoted as CS1, CS2, and CS3, and two different DM cell groups are denoted as CD1 and CD2. The same DM and different DM cell groups are shown in Table 6.

Table 6. Same and Different DM cell Groups.

				Same DM Cell Group			
CS1	Cell L	Cell M	Cell N	Cell O			
CS2	Cell A	Cell B	Cell E	Cell F			
CS3	Cell H	Cell P	Cell Q	Cell R	Cell S	Cell T	Cell V
				Different DM cell Group			
CD1	Cell C	Cell D	Cell J	Cell I			
CD2	Cell G	Cell K	Cell U				

If all the cells with similar SoH and DM are put into the same pack for a second-life application, and therefore, exposed to the same duty cycle, it is assumed their degradation will be the same. However, previous literature [3,48] suggests that cells with similar ageing history are expected to provide similar life or performance in the second-life application. Table 5 suggest that SoH and DM of the Cells A, B, D, E, F, and K, Cells H, P-T, and V, and Cells L-O are similar. Therefore, it is expected that the second-life performance of these cells will be similar. In contrast, DM of the Cells C, D, J, and I, and, Cells G, K, and U is different. Hence, it is expected that the second-life performance of these cells will be different. This cell grouping is required to check the second-life performance of the same and different DM cell groups (data generation of the second-life performance is still going on).

6. Correlation with EIS and DV Curve

EIS does not provide any peaks; thus, peak-by-peak validation is not is not a possible way to utilise the EIS data. EIS results can reveal the overall DM of the cells. Thus, to observe the similarities and dissimilarities among the EIS results of the cells, their DM were quantified by another technique developed by another research group [27]. The technique utilises Equations (3) and (4) to obtain the growth of DM (i.e., the growth of %LLI and %LAM).

While utilising the same dataset as IC, the peaks of DVA indicate different physical processes within the cell [14]. If the existing DM detection technique by DV curve can be modified in the same manner as the DM detection technique by IC curve, then the DM of each IC peak might be validated using the updated DV curve approach. Due to the limitation (flat region c.f. Section 3.1) of the DV curve technique, it is challenging to modify the current DM detection technique of the DV curve. Henceforth, the DV curve also could not verify the DM of each peak of the IC curves. However, it is difficult to verify the IC peak's DM by using EIS and DV techniques. Thus, the authors tried to determine any similarities among the EIS data and DV curves of the same DM cell group. This article grouped cells based on the first-life SoH and DM. Therefore, it is assumed that there might be similarities among the first-life EIS data and the DV curve of the same DM cell group. Alternately, differences between the 1st life EIS data and the DV curve of the different DM cell groups are anticipated. Similarities in the EIS data and DV curve may indicate a similar physical change at the first life.

6.1. EIS Data Analysis

The growth of LLI and LAM calculated from the EIS data for the cells of the same DM group (CS1 and CS2) is given in Table 7. EIS data are collected at 50% SoC. In Table 7, %LLI

and %LAM are calculated from the variations of the R_{sei}, R_{ct}, and R_w resistance at the new and aged conditions. Equations (3) and (4) (c.f. Section 3.1) are used to estimate the %LLI and %LAM from the EIS data. Nyquist plot of the cells presented in Tables 7 and 8 are provided in Figure 5.

Table 7. EIS data of the cells for the same DM group.

	CS1				CS2			
%SoC	**Cell**	**LLI% (EIS)**	**LAM% (EIS)**	**Ratio of LAM and LLI**	**Cell**	**LLI% (EIS)**	**LAM% (EIS)**	**Ratio of LAM and LLI**
50%	L	30.422	272.73	8.93	A	94.59	125.64	1.32
	M	31.02	283.86	9.15	B	92.76	139.22	1.50
	N	31.76	284.97	8.97	E	101.38	100.27	0.98
	O	684.49	274.40	0.40	F	78.63	105.28	1.33

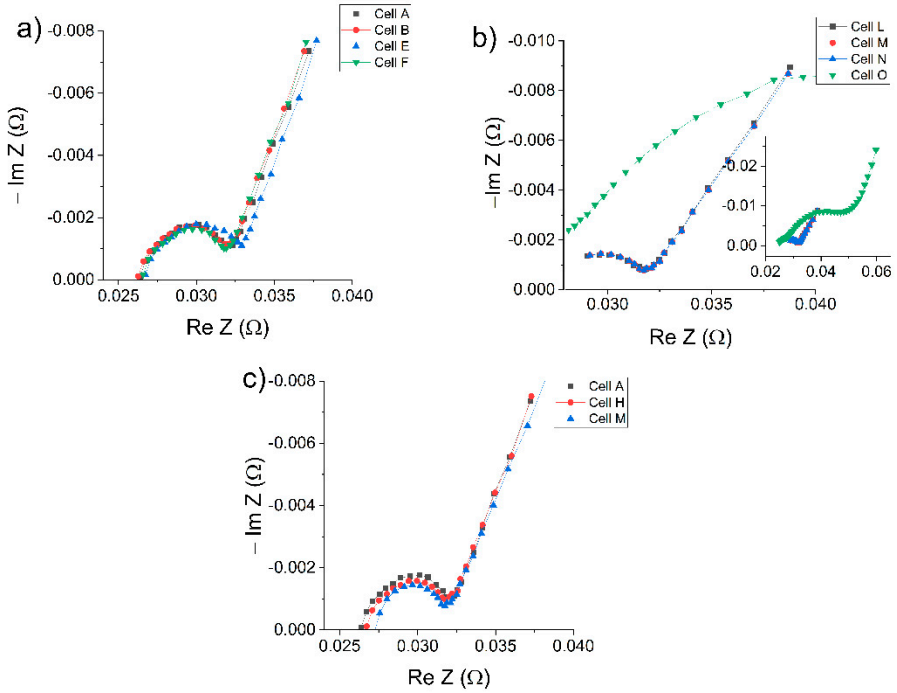

Figure 5. Nyquist plot for (**a**) CS1 (**b**) CS2 and (**c**) Different DM cells.

Similar DM is identified for the cell L, M, N, and O by IC curve analysis. EIS data of these three cells also suggest that, the ratio of LLI and LAM of these three cells is approximately the same. Although the DM of Cell O is identical to those of Cells L, M, and N, the EIS data of this cell differ from those of the other cells in this group. This discrepancy may be due to a measurement error during the EIS test of this Cell O. Nyquist plot of Cell O (Figure 5b) supports this suspicion, which shows an unusual shape of the Nyquest plot, likely due to a faulty EIS cable. As the EIS test was done using an automated process, this was not identified (and rectified) during the experiment. Furthermore, the study of IC curves revealed similar DM for Cells A, B, E, and F. The EIS results for these four cells indicate that the LAM growth rate is greater for all four cells (c.f. Table 7). The ratio of LLI to LAM is almost similar in all four cells. In short, using the modified DM identification technique, the cells determined to be identical DM cells also provide similar DM growth (e.g., for Cells L, M, and N, the ratio of LAM and LLI is nearly 9; for Cells A, B, E, and F, the ratio of LAM and LLI is nearly 1) using the EIS technique developed by other researchers [27].

Table 8 displays that DM of Cells M, A, and H are different. Though the DM of Cells M, A, and H are different, the ratio of LAM and LLI is very close for Cells A and

H. Nevertheless, EIS data of these three cells suggest that their %LLI and %LAM are significantly different. In short, using the modified DM identification technique, the cells determined to be different DM cells also provide different DM growth using the EIS technique developed by other researchers [27].

Table 8. EIS data of the cells for different DM groups.

%SoC	Cell	LLI% (EIS)	LAM% (EIS)	Ratio of LAM and LLI
50%	M	31.02	283.86	9.15
	A	94.59	125.64	1.32
	H	53.366	80.806	1.51

EIS data indicate that the resistance variance (% LLI and % LAM are estimated from R_{sei}, R_{ct}, and R_w of the EIS result) is almost similar for cells with the same DM and distinct for cells with different DM. Similarities in the ratio of the LLI and LAM indicate that there are similarities among the resistances (R_{sei}, R_{ct}, and R_w) of the cells of the same DM group. Similarities among the resistance values might be an indication of the similar physical changes in their previous life. Although the results of the EIS and IC curve are not directly correlated, there are a few similarities in the EIS data for cells within the same DM group.

6.2. DV Analysis

To validate the IC curve analysis, DV curve of the same and different DM cells are analysed. However, a visual inspection of the IC-DV curve of the same and different DM cell groups may provide useful information regarding the similarities and dissimilarities of the IC-DV curves. Thus, IC-DV curves of the cells provided in Table 6 are plotted in Section 6.2. Further analysis of the DV curves is performed by observing the changes in the DV peak positions (x-axis, y-axis). Figure 6 represents that the X-axis of the DV curve is the capacity (Q) and Y-axis is dV/dQ. Figure 5 also represents that the peak positions of the DV curves are P1, P2, and P3. One way to observe the changes in the DV peaks is to observe the peak change from new conditions to aged conditions. However, peaks in the DV curves are not as sharp as IC peaks; thus, it is difficult to identify the peak changes from new conditions to aged conditions. Therefore, the authors tried to identify the standard deviation (SD) of the aged cells' DV peak (P1, P2 and P3) positions for the cells with the same and different DM.

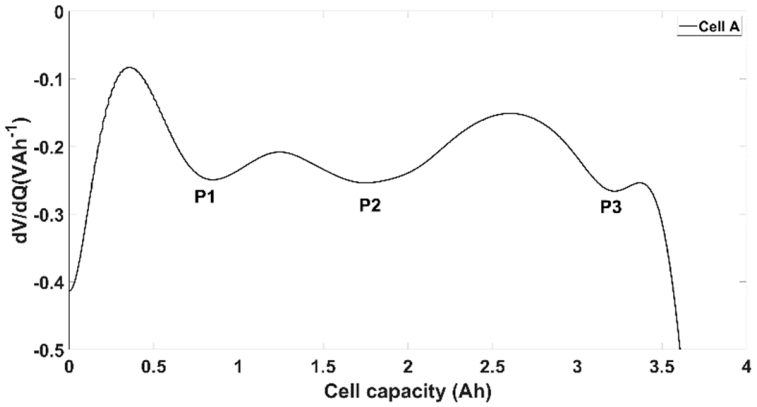

Figure 6. DV curve with peak position for Cell A.

Figures 7 and 8 represent the IC-DV curves of the same and different DM cell group. Observing the IC and DV curves in Figures 7 and 8, it is clear that, while cells have similar DM, their IC and DV curves are visually same. In contrast, the pattern varies for different DM cells. Red and purple circle of the IC-DV curve (in Figure 8) respectively, represents the uneven peaks. The magnified view of those uneven peaks are displayed in Figure 9. A similar IC—DV curve is a sign of similar physical changes [14,15]. Thus, a similar IC curve of the cells from the same DM cell groups indicates their physical changes were similar in their first life.

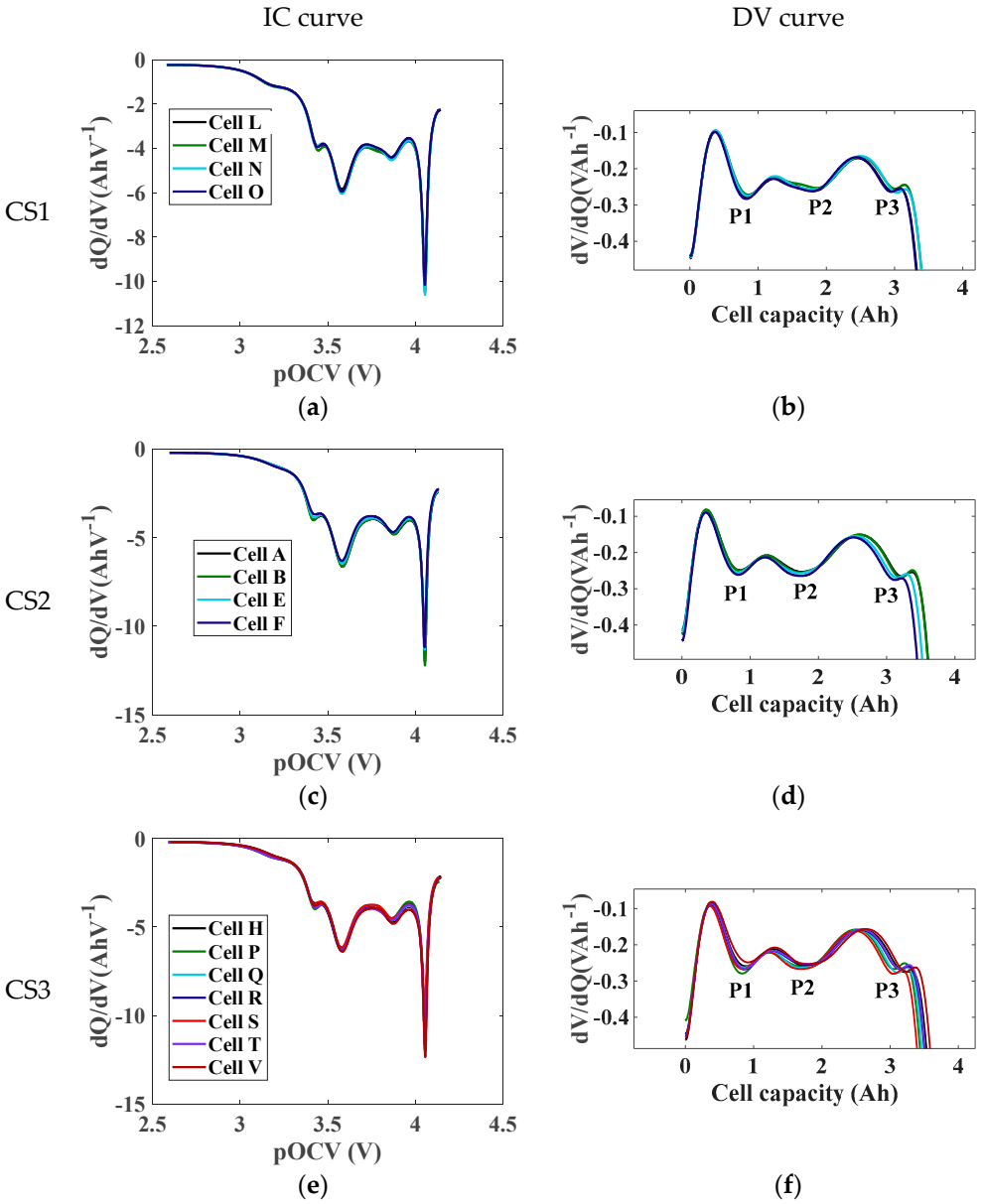

Figure 7. IC-DV curve of the Same DM cell group (**a**) IC (**b**) DV curve of L, M, N & O (**c**) IC (**d**) DV curve of A, B, E & F (**e**) IC (**f**) DV curve of H, P, Q, R, S, T & V.

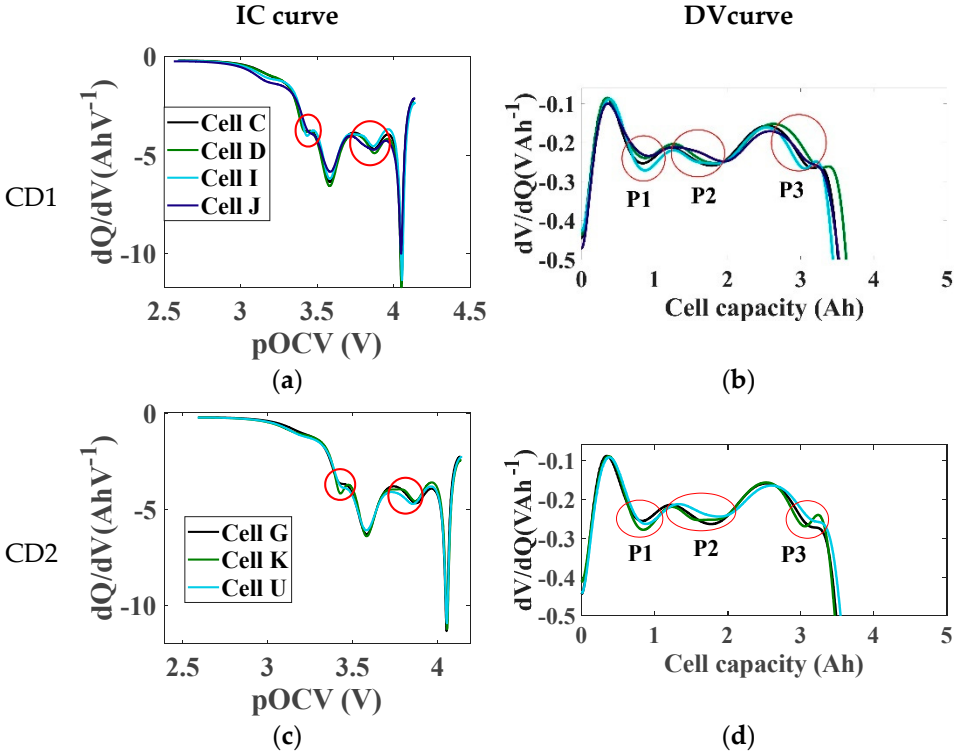

Figure 8. IC-DV curve of different DM cell groups (**a**) IC (**b**) DV curve of cell Cell C, D, I & J (**c**) IC (**d**) DV curve of Cell G, K & U.

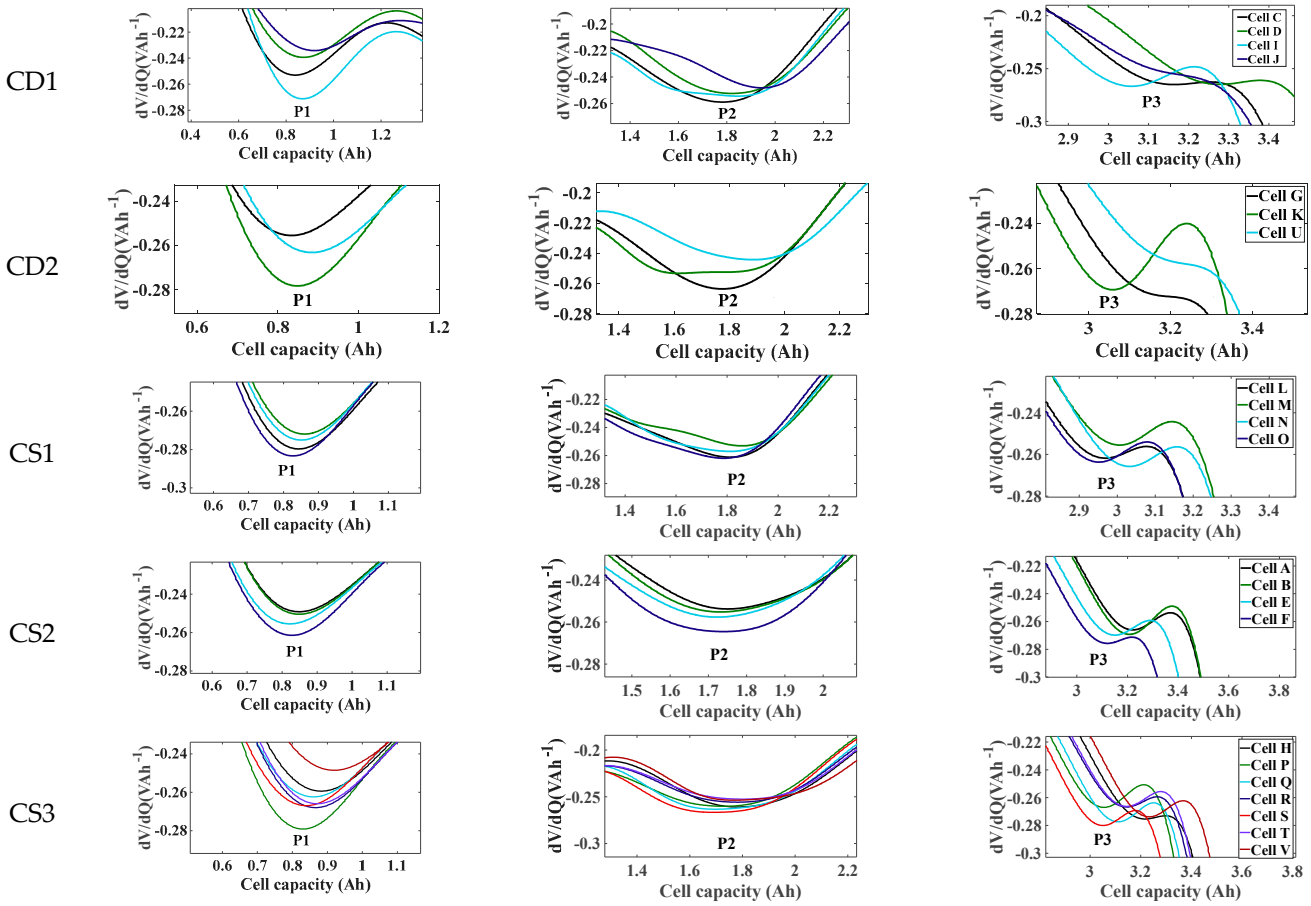

Figure 9. Magnified view of the DV curves.

Standard Deviation (SD) of the P1, P2, and P3 of the DV curves shown in Figures 7 and 8 are provided in Table 9. In Table 9, Q_{80}_SD and dV/dQ_{80}_SD define the SD of the capacity (X-axis) and SD of dV/dQ_{80} (Y-axis), respectively, at the end of their first life. The SD of the capacity and dV/dQ_{80} are calculated by using Equation (6).

$$\mathbf{SD} = \sqrt{\frac{\sum(\mathbf{x_i} - \boldsymbol{\mu})^2}{\mathbf{N}}} \quad (6)$$

$\mathbf{x_i}$ = the ith value in the data set

μ = the population mean

N = the total number of observations. Here **i** = 1,2,3 or 4 and **N** = 3 or 4 (depending on the cell number in group)

Table 9. Standard deviation of the peak positions (P-1, P-2 and P-3) of the cells.

		Q_{80}_SD (x-Axis)	dV/dQ_{80}_SD (y-Axis)
CS1	P1	0.013	0.004
	P2	0.029	0.003
	P3	0.032	0.003
CS2	P1	0.010	0.005
	P2	0.011	0.004
	P3	0.041	0.003
CS3	P1	0.026	0.009
	P2	0.039	0.005
	P3	0.063	0.005
CD1	P1	0.031	0.014
	P2	0.067	0.004
	P3	0.082	0.001
CD2	P1	0.021	0.009
	P2	0.116	0.008
	P3	0.072	0.006

Table 9 shows that Q_{80}_SD of the P2 for CS-1, CS-2, and CS-3 is 0.029, 0.011, and 0.039, respectively, whereas P2 for CD1 and CD2 are 0.067 and 0.116. This finding indicates that the standard deviation is smaller for the same DM cell group and larger for the distinct DM cell groups. Moreover, similar behaviour is also noticed for P3; Q_{80} SD is lower for identical DM cell groups and greater for different DM cell groups. Figure 9 depicts a magnified view of P1, P2, and P3 for the purpose of elucidating the variance in SD across cells with the same and different DM. Figure 9 demonstrates that the peak locations of the different DM cell groups (CD1 and CD2) differ from those of the same DM cell groupings (CS1, CS2 and CS3). These uneven peaks (refer to Figure 8) of the DV might indicate that cells in the different DM cell groups experienced different physical changes in their first life. In contrast, smooth peaks are noticed for the same DM cell groups in Figure 8. These smooth peaks of the DV curve might indicate that cells in the same DM cell groups experienced similar physical changes in the first life.

7. Further Work

The EIS and DV curve analysis presented here correlates with the modified DM identification technique (IC curve) results. However, the validation of the modified DM identification technique is still required. Ex-situ post-mortem analysis, such as SEM, EDS, and XRD, can be employed to quantify such inaccuracies and corroborate the data obtained. Moreover, in this work, EIS was performed on only nine cells. To obtain better confidence in the correlation between EIS and improved DM identification technique, EIS needs to be performed on more cells. The modified DM identification technique is applied only on LGM-50 (NMC 811 positive electrode and bi-component Graphite-SiOx negative electrode) cells. However, the technique might be applicable to other cell chemistry and format

after changing the threshold limit. In addition, the proposed modified DM identification technique can be automated and scalable to the system level; further work is going on to make the system automated and scalable.

8. Conclusions

This study correlates the updated DM identification approach with the EIS and DV analyses. The improved DM identification method was developed based on the analysis of the IC curve. The authors attempted to correlate EIS and DV data with modified DM identification-technique findings. The comparison indicates that cells identified as similar (or different) DM cells by a modified DM identification method exhibit almost similar (or different) DM growth while being assessed with the EIS technique. Additionally, the SD of the DV peaks is smaller for cells with identical DM. The cells identified as different DM cells (by a modified DM identification approach) have an EIS-obtained resistance variation that differs from that of the cells classified as the same DM cell. In addition, the SD of the DV peaks is greater for cells with different DM.

Author Contributions: Conceptualization, S.T.M., A.B. and J.M.; methodology, S.T.M.; software, A.G. and S.T.M.; formal analysis, S.T.M.; investigation, S.T.M.; data curation, S.T.M. and A.G.; writing—original draft preparation, S.T.M.; writing—review and editing, S.T.M., A.B. and J.M.; visualization, S.T.M.; supervision, A.B. and J.M. All authors have read and agreed to the published version of the manuscript.

Funding: This research received no external funding and the APC was waived by Batteries.

Institutional Review Board Statement: Not applicable.

Informed Consent Statement: Not applicable.

Data Availability Statement: Not applicable.

Conflicts of Interest: The authors declare no conflict of interest.

References

1. Casals, L.C.; García, B.A.; Canal, C. Second life batteries lifespan: Rest of useful life and environmental analysis. *J. Environ. Manag.* **2019**, *232*, 354–363. [CrossRef] [PubMed]
2. Hawkins, T.R.; Singh, B.; Majeau-Bettez, G.; Strømman, A.H. Comparative Environmental Life Cycle Assessment of Conventional and Electric Vehicles. *J. Ind. Ecol.* **2013**, *17*, 53–64. [CrossRef]
3. Martinez-Laserna, E.; Sarasketa-Zabala, E.; Sarria, I.V.; Stroe, D.-I.; Swierczynski, M.; Warnecke, A.; Timmermans, J.-M.; Goutam, S.; Omar, N.; Rodriguez, P. Technical Viability of Battery Second Life: A Study from the Ageing Perspective. *IEEE Trans. Ind. Appl.* **2018**, *54*, 2703–2713. [CrossRef]
4. SMMT Driving the Motor Industry. Car Registration. Available online: https://www.smmt.co.uk/vehicle-data/car-registrations/ (accessed on 5 November 2022).
5. Parry, T.; Department for Transport, UK. Vehicle Licensing Statistics: Annual 2018. 2019. Available online: https://assets.publishing.service.gov.uk/government/uploads/system/uploads/attachment_data/file/800502/vehicle-licensing-statistics-2018.pdf (accessed on 1 November 2022).
6. Cluzel, C.; Element Energy Ltd. Batteries on Wheels: The Role of Battery Electric Cars in the EU Power System and Beyond. Available online: http://www.element-energy.co.uk/wordpress/wp-content/uploads/2019/06/20190604_Element-Energy_Battery-study_launch-event-Final.pdf (accessed on 3 November 2022).
7. Hendrickson, T.P.; Kavvada, O.; Shah, N.; Sathre, R.; Scown, C.D. Life-cycle implications and supply chain logistics of electric vehicle battery recycling in California. *Environ. Res. Lett.* **2015**, *10*, 014011. [CrossRef]
8. Neubauer, J.S.; Wood, E.; Pesaran, A. A second life for electric vehicle batteries: Answering questions on battery degradation and value. *SAE Int. J. Mater. Manuf.* **2015**, *8*, 544–553. [CrossRef]
9. Schuster, S.F.; Brand, M.J.; Berg, P.; Gleissenberger, M.; Jossen, A. Lithium-ion cell-to-cell variation during battery electric vehicle operation. *J. Power Sources* **2015**, *297*, 242–251. [CrossRef]
10. Ungurean, L.; Cârstoiu, G.; Micea, M.V.; Groza, V. Battery state of health estimation: A structured review of models, methods and commercial devices. *Int. J. Energy Res.* **2017**, *41*, 151–181. [CrossRef]
11. Barré, A.; Deguilhem, B.; Grolleau, S.; Gérard, M.; Suard, F.; Riu, D. A review on lithium-ion battery ageing mechanisms and estimations for automotive applications. *J. Power Sources* **2013**, *241*, 680–689. [CrossRef]
12. Foster, M.; Isely, P.; Standridge, C.R.; Hasan, M.M. Feasibility assessment of remanufacturing, repurposing, and recycling of end of vehicle application lithium-ion batteries. *J. Ind. Eng. Manag. (JIEM)* **2014**, *7*, 698–715. [CrossRef]

13. Wu, B.; Yufit, V.; Merla, Y.; Martinez-Botas, R.F.; Brandon, N.P.; Offer, G.J. Differential thermal voltammetry for tracking of degradation in lithium-ion batteries. *J. Power Sources* **2015**, *273*, 495–501. [CrossRef]
14. Barai, A.; Uddin, K.; Dubarry, M.; Somerville, L.; McGordon, A.; Jennings, P.; Bloom, I. A comparison of methodologies for the non-invasive characterisation of commercial Li-ion cells. *Prog. Energy Combust. Sci.* **2019**, *72*, 1–31. [CrossRef]
15. Dubarry, M.; Devie, A.; Liaw, B.Y. The value of battery diagnostics and prognostics. *J. Energy Power Sources* **2014**, *1*, 242–249.
16. Mowri, S.T.; Barai, A.; Gupta, A.; Marco, J. Modification of Degradation Mechanism Identification Technique for Cell Grading. In Proceedings of the 2021 IEEE Vehicle Power and Propulsion Conference (VPPC), Gijon, Spain, 25–28 October 2021; pp. 1–7. [CrossRef]
17. Farmann, A.; Waag, W.; Marongiu, A.; Sauer, D.U. Critical review of on-board capacity estimation techniques for lithium-ion batteries in electric and hybrid electric vehicles. *J. Power Sources* **2015**, *281*, 114–130. [CrossRef]
18. Pastor-Fernández, C.; Bruen, T.; Widanage, W.D.; Gama-Valdez, M.A.; Marco, J. A Study of Cell-to-Cell Interactions and Degradation in Parallel Strings: Implications for the Battery Management System. *J. Power Sources* **2016**, *329*, 574–585. [CrossRef]
19. Andre, D.; Appel, C.; Soczka-Guth, T.; Sauer, D.U. Advanced mathematical methods of SOC and SOH estimation for lithium-ion batteries. *J. Power Sources* **2013**, *224*, 20–27. [CrossRef]
20. Belt, J.R.; Ho, C.D.; Motloch, C.G.; Miller, T.J.; Duong, T.Q. A capacity and power fade study of Li-ion cells during life cycle testing. *J. Power Sources* **2003**, *123*, 241–246. [CrossRef]
21. Uddin, K.; Perera, S.; Widanage, W.D.; Somerville, L.; Marco, J. Characterising Lithium-Ion Battery Degradation through the Identification and Tracking of Electrochemical Battery Model Parameters. *Batteries* **2016**, *2*, 13. [CrossRef]
22. Vetter, J.; Novák, P.; Wagner, M.R.; Veit, C.; Möller, K.-C.; Besenhard, J.O.; Winter, M.; Wohlfahrt-Mehrens, M.; Vogler, C.; Hammouche, A. Ageing mechanisms in lithium-ion batteries. *J. Power Sources* **2005**, *147*, 269–281. [CrossRef]
23. Dubarry, M.; Truchot, C.; Liaw, B.Y. Synthesise battery degradation modes via a diagnostic and prognostic model. *J. Power Sources* **2012**, *219*, 204–216. [CrossRef]
24. Birkl, C.R.; Roberts, M.R.; McTurk, E.; Bruce, P.G.; Howey, D.A. Degradation diagnostics for lithium ion cells. *J. Power Sources* **2017**, *341*, 373–386. [CrossRef]
25. Marongiu, A.; Nlandi, N.; Rong, Y.; Sauer, D.U. On-board capacity estimation of lithium iron phosphate batteries by means of half-cell curves. *J. Power Sources* **2016**, *324*, 158–169. [CrossRef]
26. Pastor-Fernández, C.; Yu, T.F.; Widanage, W.D.; Marco, J. Critical review of non-invasive diagnosis techniques for quantification of degradation modes in lithium-ion batteries. *Renew. Sustain. Energy Rev.* **2019**, *109*, 138–159. [CrossRef]
27. Pastor-Fernández, C.; Uddin, K.; Chouchelamane, G.H.; Widanage, W.D.; Marco, J. A Comparison between Electrochemical Impedance Spectroscopy and Incremental Capacity-Differential Voltage as Li-ion Diagnostic Techniques to Identify and Quantify the Effects of Degradation Modes within Battery Management Systems. *J. Power Sources* **2017**, *360*, 301–318. [CrossRef]
28. Pastor-Fernández, C.; Widanage, W.D.; Marco, J.; Gama-Valdez, M.; Chouchelamane, G.H. Identification and quantification of ageing mechanisms in Lithium-ion batteries using the EIS technique. In Proceedings of the 2016 IEEE Transportation Electrification Conference and Expo (ITEC), Dearborn, MI, USA, 27–29 June 2016; pp. 1–6. [CrossRef]
29. Abraham, D.P.; Poppen, S.D.; Jansen, A.N.; Liu, J.; Dees, D.W. Application of a lithium–tin reference electrode to determine electrode contributions to impedance rise in high-power lithium-ion cells. *Electrochim. Acta* **2004**, *49*, 4763–4775. [CrossRef]
30. Broussely, M.; Biensan, P.; Bonhomme, F.; Blanchard, P.; Herreyre, S.; Nechev, K.; Staniewicz, R. Main aging mechanisms in Li ion batteries. *J. Power Sources* **2005**, *146*, 90–96. [CrossRef]
31. Zhu, J.; Darma, M.S.D.; Knapp, M.; Sørensen, D.R.; Heere, M.; Fang, Q.; Wang, X.; Dai, H.; Mereacre, L.; Senyshyn, A.; et al. Investigation of lithium-ion battery degradation mechanisms by combining differential voltage analysis and alternating current impedance. *J. Power Sources* **2020**, *448*, 227575. [CrossRef]
32. Keil, P.; Jossen, A. Calendar Aging of NCA Lithium-Ion Batteries Investigated by Differential Voltage Analysis and Coulomb Tracking. *J. Electrochem. Soc.* **2016**, *164*, A6066–A6074. [CrossRef]
33. Dubarry, M.; Liaw, B.Y. Identify capacity fading mechanism in a commercial LiFePO4 cell. *J. Power Sources* **2009**, *194*, 541–549. [CrossRef]
34. Dubarry, M.; Liaw, B.Y.; Chen, M.-S.; Chyan, S.-S.; Han, K.-C.; Sie, W.-T.; Wu, S.-H. Identifying battery aging mechanisms in large format Li ion cells. *J. Power Sources* **2011**, *196*, 3420–3425. [CrossRef]
35. Dubarry, M.; Svoboda, V.; Hwu, R.; Liaw, B.Y. Incremental Capacity Analysis and Close-to-Equilibrium OCV Measurements to Quantify Capacity Fade in Commercial Rechargeable Lithium Batteries. *Electrochem. Solid-State Lett.* **2006**, *9*, A454–A457. [CrossRef]
36. Sarasketa-Zabala, E.; Aguesse, F.; Villarreal, I.; Rodriguez-Martinez, L.; López, C.M.; Kubiak, P. Understanding lithium inventory loss and sudden performance fade in cylindrical cells during cycling with deep-discharge steps. *J. Phys. Chem. C* **2015**, *119*, 896–906. [CrossRef]
37. Jia, X.; Zhang, C.; Zhang, L.; Zhang, W. The Degradation Characteristics and Mechanism of Li [Ni0.5Co0.2Mn0.3]O2 Batteries at Different Temperatures and Discharge Current Rates. *J. Electrochem. Soc.* **2020**, *167*, 020503. [CrossRef]
38. Stiaszny, B.; Ziegler, J.C.; Krauß, E.E.; Schmidt, J.P.; Ivers-Tiffée, E. Electrochemical characterisation and post-mortem analysis of aged $LiMn_2O_4$–Li (Ni0.5Mn0.3Co0.2)O_2/graphite lithium ion batteries. Part I: Cycle aging. *J. Power Sources* **2014**, *251*, 439–450. [CrossRef]

39. Waldmann, T.; Wilka, M.; Kasper, M.; Fleischhammer, M.; Wohlfahrt-Mehrens, M. Temperature dependent ageing mechanisms in Lithium-ion batteries—A Post-Mortem study. *J. Power Sources* **2014**, *262*, 129–135. [CrossRef]
40. Broussely, M.; Herreyre, S.; Biensan, P.; Kasztejna, P.; Nechev, K.; Staniewicz, R. Aging mechanism in Li ion cells and calendar life predictions. *J. Power Sources* **2001**, *97*, 13–21. [CrossRef]
41. Waldmann, T.; Ghanbari, N.; Kasper, M.; Wohlfahrt-Mehrens, M. Correlations between Electrochemical Data and Results from Post-Mortem Analysis of Aged Lithium-Ion Batteries. *J. Electrochem. Soc.* **2015**, *162*, A1500. [CrossRef]
42. Aurbach, D.; Markovsky, B.; Rodkin, A.; Cojocaru, M.; Levi, E.; Kim, H.-J. An analysis of rechargeable lithium-ion batteries after prolonged cycling. *Electrochim. Acta* **2002**, *47*, 1899–1911. [CrossRef]
43. Ramadass, P.; Haran, B.; White, R.; Popov, B.N. Capacity fade of Sony 18650 cells cycled at elevated temperatures: Part I. Cycling performance. *J. Power Sources* **2002**, *112*, 606–613. [CrossRef]
44. Dubarry, M.; Truchot, C.; Liaw, B.Y.; Gering, K.; Sazhin, S.; Jamison, D.; Michelbacher, C. Evaluation of commercial lithium-ion cells based on composite positive electrode for plug-in hybrid electric vehicle applications. Part II. Degradation mechanism under 2C cycle aging. *J. Power Sources* **2011**, *196*, 10336–10343. [CrossRef]
45. Podias, A.; Pfrang, A.; Di Persio, F.; Kriston, A.; Bobba, S.; Mathieux, F.; Messagie, M.; Boon-Brett, L. Sustainability Assessment of Second Use Applications of Automotive Batteries: Ageing of Li-Ion Battery Cells in Automotive and Grid-Scale Applications. *World Electr. Veh. J.* **2018**, *9*, 24. [CrossRef]
46. Wood, E.; Alexander, M.; Bradley, T.H. Investigation of battery end-of-life conditions for plug-in hybrid electric vehicles. *J. Power Sources* **2011**, *196*, 5147–5154. [CrossRef]
47. Huang, S.-C.; Tseng, K.-H.; Liang, J.-W.; Chang, C.-L.; Pecht, M.G. An Online SOC and SOH Estimation Model for Lithium-Ion Batteries. *Energies* **2017**, *10*, 512. [CrossRef]
48. Martinez-Laserna, E.; Sarasketa-Zabala, E.; Stroe, D.-I.; Swierczynski, M.; Warnecke, A.; Timmermans, J.M.; Goutam, S.; Rodriguez, P. Evaluation of lithium-ion battery second life performance and degradation. In Proceedings of the ECCE 2016—IEEE Energy Conversion Congress and Exposition, Milwaukee, WI, USA, 18–22 September 2016; IEEE: Washington, DC, USA, 2016; pp. 1–7.